


















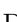

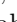









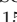


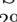



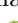


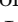




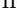
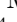


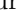

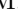

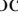
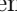



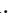
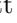
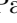











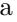

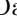





Galaxy Tomography with the Gravitational Wave Background from Supermassive Black Hole Binaries

Yifan Chen ^{1,*} Matthias Daniel,² Daniel J. D’Orazio ^{1,3} Andrea Mitridate ⁴ Laura Sagunski ² Xiao Xue ^{5,6,4,†} Gabriella Agazie ⁷ Jeremy G. Baier ⁸ Paul T. Baker ⁹ Bence Bécsy ⁸ Laura Blecha ¹⁰ Adam Brazier ^{11,12} Paul R. Brook ¹³ Sarah Burke-Spolaor ^{14,15,‡} Rand Burnette,⁸ J. Andrew Casey-Clyde ¹⁶ Maria Charisi ¹⁷ Shami Chatterjee ¹¹ Tyler Cohen ¹⁸ James M. Cordes ¹¹ Neil J. Cornish ¹⁹ Fronefield Crawford ²⁰ H. Thankful Cromartie ²¹ Megan E. DeCesar ²² Paul B. Demorest ²³ Heling Deng,⁸ Lankeswar Dey ^{14,15} Timothy Dolch ^{24,25} Elizabeth C. Ferrara ^{26,27,28} William Fiore ^{14,15} Emmanuel Fonseca ^{14,15} Gabriel E. Freedman ⁷ Emiko C. Gardiner ²⁹ Kyle A. Gersbach,¹⁷ Joseph Glaser ^{14,15} Deborah C. Good ³⁰ Kayhan Gültekin ³¹ Jeffrey S. Hazboun ⁸ Ross J. Jennings ^{14,15,§} Aaron D. Johnson ^{7,32} David L. Kaplan ⁷ Luke Zoltan Kelley ²⁹ Joey S. Key ³³ Nima Laal ⁸ Michael T. Lam ^{34,35,36} William G. Lamb ¹⁷ Bjorn Larsen,³⁷ T. Joseph W. Lazio,³⁸ Natalia Lewandowska ³⁹ Tingting Liu ^{14,15} Jing Luo ^{40,¶} Ryan S. Lynch ⁴¹ Chung-Pei Ma ^{29,42} Dustin R. Madison ⁴³ Alexander McEwen ⁷ James W. McKee ⁴⁴ Maura A. McLaughlin ^{14,15} Patrick M. Meyers ³² Chiara M. F. Mingarelli ³⁷ David J. Nice ⁴⁵ Stella Koch Ocker ^{32,46} Ken D. Olum ⁴⁷ Timothy T. Pennucci ⁴⁸ Polina Petrov ¹⁷ Nihan S. Pol ⁴⁹ Henri A. Radovan ⁵⁰ Scott M. Ransom ⁵¹ Paul S. Ray ⁵² Joseph D. Romano ⁴⁹ Jessie C. Runnoe ¹⁷ Alexander Saffer ^{51,§} Shashwat C. Sardesai ⁷ Kai Schmitz ⁵³ Xavier Siemens ^{8,7} Joseph Simon ^{54,**} Magdalena S. Siwek ⁵⁵ Sophia V. Sosa Fiscella ^{35,36} Ingrid H. Stairs ⁵⁶ Daniel R. Stinebring ⁵⁷ Abhimanyu Susobhanan ⁵⁸ Joseph K. Swiggum ^{45,§} Jacob Taylor,⁸ Stephen R. Taylor ¹⁷ Jacob E. Turner ⁴¹ Caner Unal ^{59,60,61} Michele Vallisneri ^{38,32} Rutger van Haasteren ⁵⁸ Joris Verbiest,⁶² Sarah J. Vigeland ⁷ Caitlin A. Witt ^{63,64} David Wright ⁸ and Olivia Young ^{35,36}

(The NANOGrav Collaboration)

¹Niels Bohr International Academy, Niels Bohr Institute, Blegdamsvej 17, 2100 Copenhagen, Denmark

²Institute for Theoretical Physics, Goethe University, 60438 Frankfurt am Main, Germany

³Space Telescope Science Institute, 3700 San Martin Drive, Baltimore, MD 21218, USA

⁴Deutsches Elektronen-Synchrotron DESY, Notkestr. 85, 22607 Hamburg, Germany

⁵Institut de Física d’Altes Energies (IFAE), The Barcelona Institute of Science and Technology, Campus UAB, 08193 Bellaterra (Barcelona), Spain

⁶II. Institute of Theoretical Physics, Universität Hamburg, 22761 Hamburg, Germany

⁷Center for Gravitation, Cosmology and Astrophysics, Department of Physics, University of Wisconsin-Milwaukee, P.O. Box 413, Milwaukee, WI 53201, USA

⁸Department of Physics, Oregon State University, Corvallis, OR 97331, USA

⁹Department of Physics and Astronomy, Widener University, One University Place, Chester, PA 19013, USA

¹⁰Physics Department, University of Florida, Gainesville, FL 32611, USA

¹¹Cornell Center for Astrophysics and Planetary Science and Department of Astronomy, Cornell University, Ithaca, NY 14853, USA

¹²Cornell Center for Advanced Computing, Cornell University, Ithaca, NY 14853, USA

¹³Institute for Gravitational Wave Astronomy and School of Physics and Astronomy, University of Birmingham, Edgbaston, Birmingham B15 2TT, UK

¹⁴Department of Physics and Astronomy, West Virginia University, P.O. Box 6315, Morgantown, WV 26506, USA

¹⁵Center for Gravitational Waves and Cosmology, West Virginia University, Chestnut Ridge Research Building, Morgantown, WV 26505, USA

¹⁶Department of Physics, University of Connecticut, 196 Auditorium Road, U-3046, Storrs, CT 06269-3046, USA

¹⁷Department of Physics and Astronomy, Vanderbilt University, 2301 Vanderbilt Place, Nashville, TN 37235, USA

¹⁸Department of Physics, New Mexico Institute of Mining and Technology, 801 Leroy Place, Socorro, NM 87801, USA

¹⁹Department of Physics, Montana State University, Bozeman, MT 59717, USA

²⁰Department of Physics and Astronomy, Franklin & Marshall College, P.O. Box 3003, Lancaster, PA 17604, USA

²¹National Research Council Research Associate,

National Academy of Sciences, Washington, DC 20001,

USA resident at Naval Research Laboratory, Washington, DC 20375, USA

²²George Mason University, Fairfax, VA 22030, resident at the U.S. Naval Research Laboratory, Washington, DC 20375, USA

²³National Radio Astronomy Observatory, 1003 Lopezville Rd., Socorro, NM 87801, USA

²⁴Department of Physics, Hillsdale College, 33 E. College Street, Hillsdale, MI 49242, USA

²⁵Eureka Scientific, 2452 Delmer Street, Suite 100, Oakland, CA 94602-3017, USA

²⁶Department of Astronomy, University of Maryland, College Park, MD 20742, USA

²⁷Center for Research and Exploration in Space Science and Technology, NASA/GSFC, Greenbelt, MD 20771

- ²⁸*NASA Goddard Space Flight Center, Greenbelt, MD 20771, USA*
- ²⁹*Department of Astronomy, University of California, Berkeley, 501 Campbell Hall #3411, Berkeley, CA 94720, USA*
- ³⁰*Department of Physics and Astronomy, University of Montana, 32 Campus Drive, Missoula, MT 59812*
- ³¹*Department of Astronomy and Astrophysics, University of Michigan, Ann Arbor, MI 48109, USA*
- ³²*Division of Physics, Mathematics, and Astronomy, California Institute of Technology, Pasadena, CA 91125, USA*
- ³³*University of Washington Bothell, 18115 Campus Way NE, Bothell, WA 98011, USA*
- ³⁴*SETI Institute, 339 N Bernardo Ave Suite 200, Mountain View, CA 94043, USA*
- ³⁵*School of Physics and Astronomy, Rochester Institute of Technology, Rochester, NY 14623, USA*
- ³⁶*Laboratory for Multiwavelength Astrophysics, Rochester Institute of Technology, Rochester, NY 14623, USA*
- ³⁷*Department of Physics, Yale University, New Haven, CT 06520, USA*
- ³⁸*Jet Propulsion Laboratory, California Institute of Technology, 4800 Oak Grove Drive, Pasadena, CA 91109, USA*
- ³⁹*Department of Physics and Astronomy, State University of New York at Oswego, Oswego, NY 13126, USA*
- ⁴⁰*Department of Astronomy & Astrophysics, University of Toronto, 50 Saint George Street, Toronto, ON M5S 3H4, Canada*
- ⁴¹*Green Bank Observatory, P.O. Box 2, Green Bank, WV 24944, USA*
- ⁴²*Department of Physics, University of California, Berkeley, CA 94720, USA*
- ⁴³*Department of Physics, University of the Pacific, 3601 Pacific Avenue, Stockton, CA 95211, USA*
- ⁴⁴*Department of Physics and Astronomy, Union College, Schenectady, NY 12308, USA*
- ⁴⁵*Department of Physics, Lafayette College, Easton, PA 18042, USA*
- ⁴⁶*The Observatories of the Carnegie Institution for Science, Pasadena, CA 91101, USA*
- ⁴⁷*Institute of Cosmology, Department of Physics and Astronomy, Tufts University, Medford, MA 02155, USA*
- ⁴⁸*Institute of Physics and Astronomy, Eötvös Loránd University, Pázmány P. s. 1/A, 1117 Budapest, Hungary*
- ⁴⁹*Department of Physics, Texas Tech University, Box 41051, Lubbock, TX 79409, USA*
- ⁵⁰*Department of Physics, University of Puerto Rico, Mayagüez, PR 00681, USA*
- ⁵¹*National Radio Astronomy Observatory, 520 Edgemont Road, Charlottesville, VA 22903, USA*
- ⁵²*Space Science Division, Naval Research Laboratory, Washington, DC 20375-5352, USA*
- ⁵³*Institute for Theoretical Physics, University of Münster, 48149 Münster, Germany*
- ⁵⁴*Department of Astrophysical and Planetary Sciences, University of Colorado, Boulder, CO 80309, USA*
- ⁵⁵*Center for Astrophysics, Harvard University, 60 Garden St, Cambridge, MA 02138, USA*
- ⁵⁶*Department of Physics and Astronomy, University of British Columbia, 6224 Agricultural Road, Vancouver, BC V6T 1Z1, Canada*
- ⁵⁷*Department of Physics and Astronomy, Oberlin College, Oberlin, OH 44074, USA*
- ⁵⁸*Max-Planck-Institut für Gravitationsphysik (Albert-Einstein-Institut), Callinstraße 38, D-30167, Hannover, Germany*
- ⁵⁹*Department of Physics, Middle East Technical University, 06531 Ankara, Turkey*
- ⁶⁰*Department of Physics, Ben-Gurion University of the Negev, Be'er Sheva 84105, Israel*
- ⁶¹*Feza Gursey Institute, Bogazici University, Kandilli, 34684, Istanbul, Turkey*
- ⁶²*Department of Physics, University of Central Florida, Orlando, FL 32816-2385, USA*
- ⁶³*Center for Interdisciplinary Exploration and Research in Astrophysics (CIERA), Northwestern University, Evanston, IL 60208, USA*
- ⁶⁴*Adler Planetarium, 1300 S. DuSable Lake Shore Dr., Chicago, IL 60605, USA*
- (Dated: November 12, 2024)

The detection of a stochastic gravitational wave background by pulsar timing arrays suggests the presence of a supermassive black hole binary population. Although the observed spectrum generally aligns with predictions from orbital evolution driven by gravitational wave emission in circular orbits, there is a discernible preference for a turnover at the lowest observed frequencies. This turnover could indicate a significant hardening phase, transitioning from early environmental influences to later stages predominantly influenced by gravitational wave emission. In the vicinity of these binaries, the ejection of stars or dark matter particles through gravitational three-body slingshots efficiently extracts orbital energy, leading to a low-frequency turnover in the spectrum. By analyzing the NANOGrav 15-year data, we assess how the gravitational wave spectrum depends on the initial inner galactic profile prior to disruption by binary ejections, accounting for a range of initial binary eccentricities. Our findings suggest a parsec-scale galactic center density around $10^6 M_{\odot}/\text{pc}^3$ across most of the parameter space, offering insights into the environmental effects on black hole evolution and combined matter density near galaxy centers.

* Corresponding author: Yifan Chen yifan.chen@nanograv.org

† Corresponding author: Xiao Xue xxue@ifae.es

I. Introduction

Recent advances by pulsar timing arrays (PTAs), leveraging precise measurements of timing residuals within a galactic-scale detector, have ushered in a new era of stochastic gravitational wave background (SGWB) detection. The SGWB, defined by a superposition of incoherent gravitational waves (GWs), initially emerged as a common-spectrum process [1–4]. Subsequent data provided robust evidence of a quadrupolar correlation function [5–8], famously known as the Hellings-Downs curve [9], further affirming the SGWB’s presence and characteristics.

The observed spectrum of the SGWB is consistent with expectations for a population of supermassive black hole binaries (SMBHBs), dominated by binaries with comparable mass ratios, total masses in the range of $10^{9.2-10.4} M_\odot$, and redshifts from 0.15 to 0.9 [10, 11], where M_\odot represents the solar mass. Although the spectrum is consistent with a steady spectral slope driven by GW emission from circular binaries, it also suggests a low-frequency turnover [10, 12]. This feature implies an acceleration in the rate of orbital hardening, offering a potential solution to the final parsec problem [13, 14]. Possibilities include interactions with environmental factors—such as gas [15, 16], stars [17], and dark matter (DM) [18]—and the impact of significant initial orbital eccentricities [19–21].

An intriguing aspect of environmental interactions involves the role of stars and particle DM, which are noted for their potentially high density in galactic centers (GCs) [22–24]. Both stars and DM can be expelled from the system through gravitational slingshots during encounters with binary components, thereby extracting orbital energy [17]. This process involves three-body scattering, where the energy extraction efficiency is significantly higher than that of two-body dynamical friction [25], especially when the binary components have comparable masses and are sufficiently close. Such three-body slingshot interactions can substantially alter the density profile of the GC, particularly flattening the inner distribution [18, 26]. This underscores the importance of considering the co-evolution of the density profile and the binary orbit. A pivotal study by Ref. [27] demonstrates that the orbital hardening rate observed in N-body simulations can be effectively approximated by results from scattering experiments [17] within environments characterized by the GC distribution at the SMBHB influence radius [28] prior to disruption. In this

study, we examine the impact of initial GC density profiles and SMBHB eccentricities on the SGWB spectrum, utilizing NANOGrav’s 15-year dataset to constrain the parameter space of these two factors.

II. Binary Hardening by Three-body Scattering

The SGWB emanating from SMBHBs constitutes an incoherent superposition of signals from individual sources. The spectrum of this background is delineated by the characteristic strain, $h_c(f)$, as follows [19, 29]:

$$h_c^2(f) = \frac{4G}{c^2\pi f} \int dz dM dq \frac{d^3\eta}{dz dM dq} \frac{dE_{\text{GW}}}{df_s}, \quad (1)$$

where G represents the gravitational constant, and c denotes the speed of light. The GW frequency emitted in the source frame is denoted by f_s , and $f = f_s/(1+z)$, incorporating the redshift factor z . The comoving volumetric number density of SMBHBs, $d^3\eta/(dz dM dq)$, depends on the redshift z , the total binary mass M , and the mass ratio $q \leq 1$. The GW emission spectrum from a binary, $dE_{\text{GW}}/d \ln f_s$, is expressed in the context of a circular orbit as follows [30]:

$$\left. \frac{dE_{\text{GW}}}{df_s} \right|^{e=0} = -\frac{dt}{da} \frac{64}{15} \frac{\pi^{8/3}}{c^5} G^{8/3} M^{11/3} f_s^{5/3} \frac{q^2}{(1+q)^4}. \quad (2)$$

Here, a represents the semi-major axis of the orbit, adhering to Kepler’s law $a^3 = GM/(2\pi f_{\text{orb}})^2$, where the orbital frequency $f_{\text{orb}} = f_s/2$ for circular orbits. The orbital hardening process, denoted by $da/dt \equiv \sum_i da/dt|_i$, with the index i encompassing various sources of hardening [31–34], is crucial for binary evolution. The evolution of the semi-major axis due solely to GW emission in circular orbits is described as follows [35]:

$$\left. \frac{da}{dt} \right|_{\text{GW}}^{e=0} = -\frac{64}{5} \frac{G^3 M^3}{c^5 a^3} \frac{q}{(1+q)^2}, \quad (3)$$

leading to a characteristic strain $h_c \propto f^{-2/3}$. Eccentric orbits lead to enhanced GW emission over a range of frequencies, as detailed in the Supplemental Material. Consequently, a turnover in the spectrum at lower frequencies is possible before the orbit undergoes circularization through GW emission [19].

In GCs, SMBHBs form within a background of stars and particle DM, once their separation falls below the influence radius, r_i . This radius is defined as the distance at which the total enclosed mass of stars and DM equals twice the mass of the SMBHB [28]. Given their substantial mass disparity with the SMBHB, both stars and DM particles act effectively as test particles. Each may undergo multiple gravitational encounters with one of the black holes (BHs) until it gains sufficient kinetic energy to be ejected. This three-body slingshot process becomes efficient as the semi-major axis a approaches the hardening radius, defined as $a_h \equiv r_i q/(4(1+q)^2)$ [17]. The rate

‡ Sloan Fellow

§ NANOGrav Physics Frontiers Center Postdoctoral Fellow

¶ Deceased

** NSF Astronomy and Astrophysics Postdoctoral Fellow

of orbital hardening due to three-body scattering (3BS), averaged over a background of particles with matter density ρ and velocity dispersion σ , is given by [17]:

$$\left. \frac{da}{dt} \right|_{3BS} = -HG \frac{\rho}{\sigma} a^2, \quad (4)$$

where H is a dimensionless coefficient typically ranging from 15 to 20, as observed in scattering experiments [17]. It is important to note that three-body scattering is fundamentally distinct from two-body dynamical friction [25, 36–39] and becomes more dominant after entering the hardening radius. Assuming a constant ρ/σ ratio over time, the spectral evolution for circular orbits follows $h_c \propto f$. Note that three-body scatterings tend to increase the eccentricity on average [17], in contrast to the effects of GW emission.

Historically, the three-body slingshot process was thought to result in stalled orbital evolution by expelling background stars and depleting a specific phase-space region known as the loss cone. This led to what is known as the final parsec problem [13]. However, N-body simulations [40–42] have shown that merger-induced triaxiality can efficiently repopulate the loss cone [43].

These simulations also reveal that two initial DM profiles, each centered around a BH with peak densities at the center, will merge and flatten into a single core profile following the merger [18, 26, 44]. This underscores the need for comprehensive simulations that simultaneously address the co-evolution of the SMBHB orbit and the density profile. Further analysis comparing results from scattering experiments [17] with N-body simulation outcomes [42] demonstrates that predictions of orbital evolution can closely align with Eq. (4), assuming that ρ/σ remains constant, determined by the initial profile at the SMBHB’s influence radius, r_i [27]. This statement is supported by observations that the total mass ejected during SMBHB evolution is approximately of the order of M [17, 18, 45, 46], primarily distributed within the influence radius at the onset. During simulations, the loss cone at this radius remains fully populated, driven by the efficient diffusion of particles.

By combining Eq. (3) and Eq. (4), the GW spectrum is revealed to exhibit two distinct phases: one at low frequencies, predominantly shaped by three-body scattering, and another at high frequencies, primarily determined by GW emission. The transition between these phases is marked by a turnover frequency in the source frame [20]:

$$\begin{aligned} f_t &= \pi^{-1} \left(\frac{5c^5}{64} \frac{(1+q)^2}{q} \frac{\rho_i}{\sigma_i} H \right)^{3/10} G^{-1/10} M^{-2/5} \\ &\approx 2.8 \text{ nHz} \left(\frac{(1+q)^2}{q} \frac{\rho_i/\bar{\rho}_{\text{ref}}}{\sigma_i/\bar{\sigma}_{\text{ref}}} \frac{H}{18} \right)^{3/10} \left(\frac{M}{10^{10} M_\odot} \right)^{-2/5}, \end{aligned} \quad (5)$$

Here, we define $\bar{\rho}_{\text{ref}} \equiv 10^5 M_\odot/\text{pc}^3 \approx 3.8 \times 10^6 c^{-2} \text{ GeV}/\text{cm}^3$ and $\bar{\sigma}_{\text{ref}} \equiv 10^{-3} c$. Figure 1 presents examples of the GW spectrum from an individual SMBHB

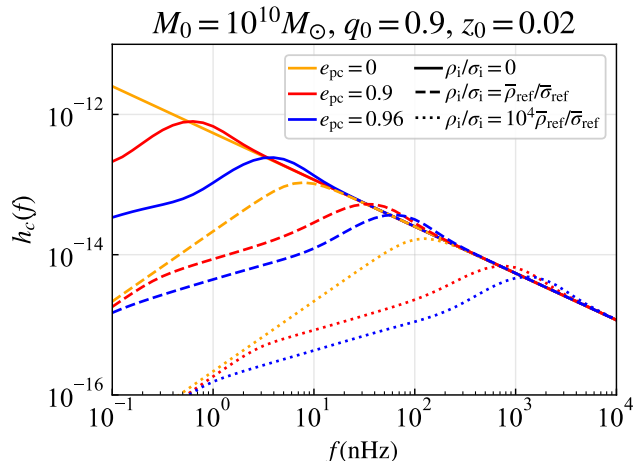


FIG. 1: Examples of the SGWB spectrum derived from an SMBHB population modeled as delta functions in the space of (M, q, z) , specifically, $d^3\eta/(dzdMdq) = \delta(M - M_0)\delta(z - z_0)\delta(q - q_0) \text{ Mpc}^{-3}$. The constant parameters (M_0, z_0, q_0) are indicated at the top. All scenarios initiate the evolution of the semi-major axis a and contribute to GW emission starting at 1 pc, with the eccentricity e_{pc} defined at this separation. Colors indicate different e_{pc} values, while line styles represent different ρ_i/σ_i for three-body scattering, with $\bar{\rho}_{\text{ref}} \equiv 10^5 M_\odot/\text{pc}^3$ and $\bar{\sigma}_{\text{ref}} \equiv 10^{-3} c$.

across various parameter settings, demonstrating how the magnitude of three-body scattering and the initial binary eccentricity influence the spectral shape.

III. Galaxy Tomography

The NANOGrav 15-year data indicates a slight preference for a turnover at low frequencies, particularly around 4 nHz [10, 12], suggesting deviations from the expected behavior of purely circular binaries driven by GW emission. Given that both eccentricity and star/DM-induced three-body scatterings can contribute to this turnover, we conduct a comprehensive survey of their joint parameter space.

We adopt a straightforward power-law distribution for the GC density profile prior to disruption, parameterized as follows:

$$\rho(r) = \rho_{\text{pc}} \left(\frac{r}{1 \text{ pc}} \right)^{-\gamma}, \quad (6)$$

where the reference radius 1 pc is set for our analysis, ρ_{pc} denotes the matter density normalization to be constrained, and γ represents the radial slope of the profile. We explore values of γ ranging from 0 to 2.5, consistent with the inner region of the Dehnen density profile family [47]. For each scenario, we first determine the influence radius r_i by satisfying the condition

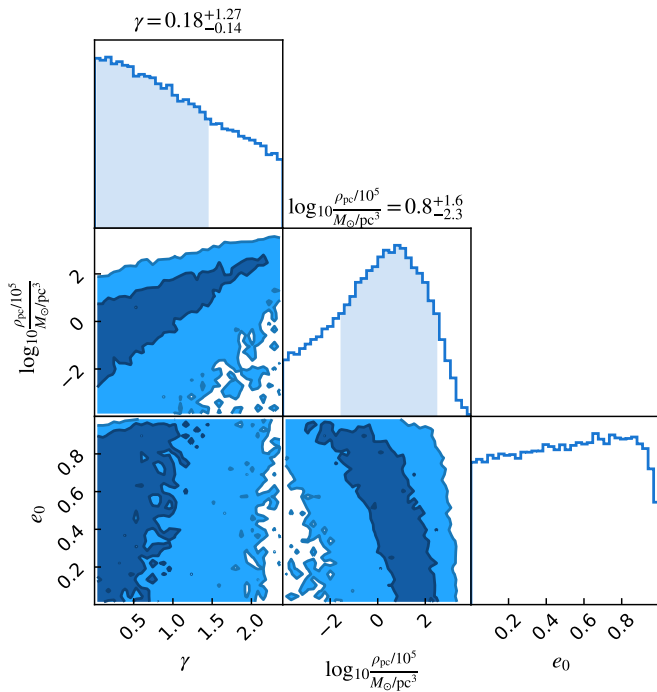


FIG. 2: Posterior distribution of the parameters $(\log_{10}(\rho_{\text{pc}}[M_{\odot}/\text{pc}^3]/10^5), \gamma)$ for the density profile prior to disruption and initial eccentricity e_0 from the lowest five frequency bins of the NANOGrav 15-year dataset. The 1σ and 2σ confidence regions are depicted in dark blue and light blue, respectively. The SMBHB population parameters used to produce the SGWB follow the fiducial ‘Phenom+Astro’ model from Ref. [10], without incorporating phenomenological environmental parameters, with normalization treated as a nuisance parameter based on astrophysical priors.

$\int_0^{r_i} \rho 4\pi r^2 dr = 2M$ [28], and then calculate $\rho_i \equiv \rho(r_i)$ using Eq. (6) and $\sigma_i \equiv \sigma(r_i) = \sqrt{GM/r_i}$ via the virial theorem.

Our analysis targets include the initial eccentricity e_0 , defined as occurring when the binary is formed at $a = r_i$, and the density profile parameters ρ_{pc} and γ . The distribution of SMBHB parameters, including total mass M , mass ratio q , and redshift z , follows the fiducial population model derived from NANOGrav’s astrophysical interpretations (fiducial ‘Phenom+Astro’ model without phenomenological environmental parameters) using `holodeck` [10]. The dominant contributions to the SGWB are expected from binaries with $\log_{10}(M/M_{\odot}) \in (9.2, 10.4)$, $q \in (0.5, 0.8)$, and $z \in (0.15, 0.9)$.

For each parameter combination of $(e_0, \rho_{\text{pc}}, \gamma)$ and (M, q, z) , we compute the orbital and eccentricity evolution of the SMBHB, taking into account both GW emission and three-body scattering, as detailed in the Supplemental Material. We then derive the total SGWB spectrum by integrating over (M, q, z) . Finally, we assess the likelihood that the SGWB spectrum, generated

from each set of parameters $(e_0, \rho_{\text{pc}}, \gamma)$, matches the lowest five frequency bins, ranging from 2 to 10 nHz, of the NANOGrav 15-year data, which exhibit robust signal-to-noise ratios [5]. We treat the overall normalization of the SMBHB distribution as a nuisance parameter, assigning it a prior derived from astrophysical priors, as detailed in Supplemental Material.

In Fig. 2, we present the posterior distribution of the parameters $(e_0, \log_{10}(\rho_{\text{pc}}[M_{\odot}/\text{pc}^3]/10^5), \gamma)$. The results reveal that the 1σ regions (dark blue) indicate the presence of three-body scatterings, with $\log_{10}(\rho_{\text{pc}}[M_{\odot}/\text{pc}^3]/10^5)$ estimated at $0.8^{+1.7}_{-2.3}$. Variations in the SMBHB population distribution would only shift this best-fit region, adhering to the scaling relations from Eq. (5). There is an expected degeneracy between e_0 and ρ_{pc} [11, 48–50], where a higher e_0 corresponds to a lower required density. However, the 1σ region indicates that when ρ_{pc} drops below $10 M_{\odot}/\text{pc}^3$, GW emission requires an extremely high initial eccentricity, $e_0 > 0.999$, to account for the turnover. This is because lower densities result in a larger r_i , and GW emission tends to circularize the orbit before it reaches the observed frequency range. The light blue regions represent the 2σ confidence interval. The white region is excluded at the 95%-confidence level, thereby setting an upper limit on ρ_{pc} as it would result in a turnover frequency inconsistent with the observational data.

In the left panel of Fig. 3, we present the posterior distribution for the density profile parameters $(\rho_{\text{pc}}, \gamma)$ for specific initial eccentricities of $e_0 = 0, 0.5$, and 0.9 . The contours generally follow approximately constant values of ρ_i/σ_i , as suggested by Eq. (5). The right panel of Fig. 3 presents the best-fit spectrum for various values of e_0 . Distributions with smaller γ values are preferred over steeper ones because larger γ leads to a broader range of ρ_i/σ_i across the SMBHB population parameters (M, q) , which in turn results in a wider distribution of the turnover frequency f_t as defined in Eq. (5). This causes the spectrum to have a broader intermediate region, requiring a normalization factor higher than the fiducial value, making high- γ cases less favored. A conservative upper limit on $\rho_{\text{pc}}(\gamma)$ is established based on the 95% exclusion for $e_0 = 0$, since higher e_0 values lead to more stringent constraints.

For comparative purposes, we examine various benchmark star and DM profiles: the modelled stellar distribution in the nearby galaxy M87 with $\gamma = 4/3$ and $\rho_{\text{pc}} \approx 0.7 \times 10^5 M_{\odot}/\text{pc}^3$ [51] (black star); the Milky Way’s (MW) modelled core star distribution with $\gamma = 1/2$ and $\rho_{\text{pc}} \approx 1.8 \times 10^5 M_{\odot}/\text{pc}^3$ [52] (yellow star); a hypothetical DM spike in M87 with $\gamma = 7/3$ and $\rho_{\text{pc}} \approx 2.6 \times 10^6 M_{\odot}/\text{pc}^3$ [23], formed by an adiabatically growing central SMBH from an initial Navarro-Frenk-White distribution [22] (brown dot); and a hypothetical flattened DM spike in the MW with $\gamma = 1/2$ and $\rho_{\text{pc}} \approx 10^4 M_{\odot}/\text{pc}^3$, formed as the BH grew from a low-mass seed [53] (orange dot). Interestingly, DM spikes are not favored in the hardening process because higher γ

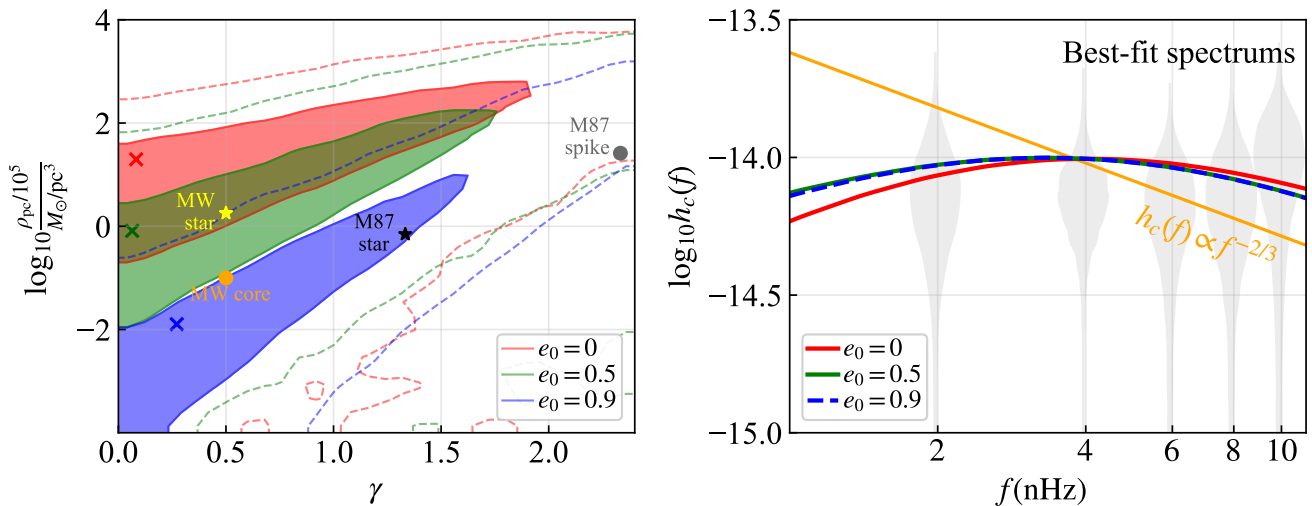


FIG. 3: **Left:** Posterior distribution of the density profile parameters ($\log_{10}(\rho_{\text{pc}}[M_{\odot}/\text{pc}^3]/10^5)$, γ) for three specific initial eccentricities: $e_0 = 0$ (blue), 0.5 (green), and 0.9 (red). The 1σ and 2σ confidence regions are depicted in darker shades and marked by dashed lines, respectively. Benchmark matter density profiles, including the star distribution in M87 (black star), the star core in the Milky Way (MW) (yellow star), a dark matter (DM) spike in M87 (gray dot), and a flattened DM core in the MW (orange dot), are presented for comparison, with detailed parameters provided in the text. **Right:** Best-fit SGWB spectrum with parameters $(\log_{10}(\rho_{\text{pc}}[M_{\odot}/\text{pc}^3]/10^5), \gamma) = (1.3, 0), (-0.09, 0.06)$, and $(-1.9, 0.27)$ for $e_0 = 0, 0.5$, and 0.9 , respectively, as indicated by the crosses (\times) in the left panel with darker colors. The spectrum is shown against the lowest five frequency bins from the NANOGrav 15-year dataset [5].

values result in larger r_i above 1 pc, leading to lower ρ_i . Conversely, the core-like star or DM distributions with $\gamma = 1/2$ align with our best-fit regions. Lower γ values are expected due to flattening by previous SMBHB mergers or reformation after a galaxy merger [53].

IV. Discussion

In the vicinity of a binary BH, a test particle can extract orbital energy through multiple scatterings with each BH component. Within the PTA observation band, the three-body ejection process is significantly more efficient than two-body dynamical friction, particularly for comparable-mass binaries, leading to pronounced back-reaction effects on the surrounding matter distribution. In this study, we explore the potential imprints that stars or particle DM surrounding SMBHBs could leave on the spectrum of the SGWB. Utilizing data from NANOGrav’s 15-year observation, we constrain the relevant parameter space. Our results support the existence of three-body scatterings with a reasonable density distribution prior to disruption (see the left panel of Fig. 2), primarily inferred from the low-frequency turnover in the SGWB spectrum, assuming no other dominant environmental influences are present. Continued monitoring with existing PTAs will provide improved constraints on the low-frequency turnover. Future observations from the Square Kilometre Array [54] and next-generation astrometry missions [55] are expected to provide signifi-

cantly more precise spectral information [56], potentially elucidating the turnover.

Another potential source of environmental effects is a circumbinary disk around the SMBHB. If the GCs hosting SMBHBs are gas-rich and the binaries are accreting at the Eddington rate, the gas-driven hardening rate (conservatively choosing large values from Ref. [57]), could be comparable to three-body scatterings at separations below 0.1 pc for $M \sim 10^{10} M_{\odot}$ (2 nHz). However, at these separations and lower the binary will decouple from the disk [58], thus mitigating disk-driven hardening. Furthermore, SMBHBs of this mass cannot be surrounded by gravitationally stable thin disks until closer to merger and massive self-gravitating disks must be employed [59–61].

To precisely determine the density profile, resolving the degeneracy with the initial eccentricity is essential. Potential strategies to determine SMBHB eccentricity include resolving individual binaries through either GW or electromagnetic observations [62, 63] and examining correlations among different frequency bins. This latter method is based on the observation that high eccentricity contributes to multiple integer multiples of frequency bins simultaneously [21]. Nevertheless, setting a stringent upper limit on the galactic center density distribution is feasible, as both additional environmental influences and nonzero orbital eccentricity tend to further elevate the turnover frequency.

The three-body slingshot mechanism considered in this study assumes that the test particles interact purely grav-

itionally, thus applying to both stars and cold, collisionless DM. If DM is the dominant density, the findings here could provide crucial insights into two long-standing questions: the identification of the particle nature of DM and the measurement of its density at galactic centers. Further investigations are needed to determine how DM models that extend beyond the test particle hypothesis—such as wave-like DM [38] or self-interacting DM [64, 65]—interact with binaries, particularly in terms of the applicability of three-body ejection or two-body dynamical friction. Notably, wave-like DM exhibits distinct behaviors depending on the binary separation scale and the boson mass [66–71]. For a star-dominant distribution, such findings could reveal the star formation and relaxation rates near SMBHs in the galactic center, suggesting a density higher than previously expected [20, 72].

Authorship Contributions

This paper uses a decade’s worth of pulsar timing observations and is the product of the work of many people.

Y.C., L.S., and X.X. initiated the project and developed the core idea, with D.J.D. contributing to its development. Y.C., M.D., D.J.D., A.M., L.S., and X.X. participated in discussions, provided critical feedback, and shaped the research and analysis. Y.C. coordinated the project and wrote the manuscript. M.D. and X.X. developed the analysis code, created figures, and edited the text. D.J.D. offered guidance on the supermassive black hole binary population model and the `holodeck` code, wrote the discussion on the environmental effects from gas, and edited the text. A.Mi. provided guidance on the `PTArcade` code and the presentation of NANOGrav 15-year data.

G.A., A.A., A.M.A., Z.A., P.T.B., P.R.B., H.T.C., K.C., M.E.D., P.B.D., T.D., E.C.F., W.F., E.F., G.E.F., N.G.D., D.C.G., P.A.G., J.G., R.J.J., M.L.J., D.L.K., M.K., M.T.L., D.R.L., J.L., R.S.L., A.M., M.A.M., N.M., B.W.M., C.N., D.J.N., T.T.N., B.B.P.P., N.S.P., H.A.R., S.M.R., P.S.R., A.S., C.S., B.J.S.A., I.H.S., K.S., A.S., J.K.S., and H.M.W. developed timing models and ran observations for the NANOGrav 15 yr data set. Development of the `holodeck` population modeling framework was led by L.Z.K., with contributions from A.C-C., D.W., E.C.G., J.M.W., K.G., M.S.S., and S.C. `PTArcade`, which was used in this analysis, was mainly developed by A.Mi., with help from D.W., K.D.O., J.N., R.v.E., T.S., and T.T.

Acknowledgments

We are grateful to Kfir Blum, Vitor Cardoso, Gregorio Carullo, James Cline, Hyungjin Kim, Bin Liu, Yiqiu Ma, Zhen Pan, and Rodrigo Vicente for useful discussions.

The NANOGrav Collaboration receives support from National Science Foundation (NSF) Physics Frontiers Center award Nos. 1430284 and 2020265, the Gordon and Betty Moore Foundation, NSF AccelNet award No. 2114721, an NSERC Discovery Grant, and CIFAR. The Arecibo Observatory is a facility of the NSF operated under cooperative agreement (AST-1744119) by the University of Central Florida (UCF) in alliance with Universidad Ana G. Méndez (UAGM) and Yang Enterprises (YEI), Inc. The Green Bank Observatory is a facility of the NSF operated under cooperative agreement by Associated Universities, Inc. The National Radio Astronomy Observatory is a facility of the NSF operated under cooperative agreement by Associated Universities, Inc. Part of this research was performed at the Jet Propulsion Laboratory, under contract with the National Aeronautics and Space Administration. Copyright 2024.

Y.C. is supported by VILLUM FONDEN (grant no. 37766), by the Danish Research Foundation, and under the European Union’s H2020 ERC Advanced Grant “Black holes: gravitational engines of discovery” grant agreement no. Gravitas–101052587. Views and opinions expressed are however those of the author only and do not necessarily reflect those of the European Union or the European Research Council. Neither the European Union nor the granting authority can be held responsible for them. D.J.D. acknowledges support from the Danish Independent Research Fund through Sapere Aude Starting Grant No. 121587. A.Mi. and X.X. are supported by the Deutsche Forschungsgemeinschaft under Germany’s Excellence Strategy - EXC 2121 Quantum Universe - 390833306. IFAE is partially funded by the CERCA program of the Generalitat de Catalunya. X.X. is funded by the grant CNS2023-143767. Grant CNS2023-143767 funded by MICIU/AEI/10.13039/501100011033 and by European Union NextGenerationEU/PRTR. Y.C. and X.X. acknowledge the support of the Rosenfeld foundation and the European Consortium for Astroparticle Theory in the form of an Exchange Travel Grant. L.B. acknowledges support from the National Science Foundation under award AST-1909933 and from the Research Corporation for Science Advancement under Cottrell Scholar Award No. 27553. P.R.B. is supported by the Science and Technology Facilities Council, grant number ST/W000946/1. S.B. gratefully acknowledges the support of a Sloan Fellowship, and the support of NSF under award #1815664. M.C. and S.R.T. acknowledge support from NSF AST-2007993. M.C. and N.S.P. were supported by the Vanderbilt Initiative in Data Intensive Astrophysics (VIDA) Fellowship. K.Ch., A.D.J., and M.V. acknowledge support from the Caltech and Jet Propulsion Laboratory President’s and Director’s Research and Development Fund. K.Ch. and A.D.J. acknowledge support from the Sloan Foundation. Support for this work was provided by the NSF through the Grote Reber Fellowship Program administered by Associated Universities, Inc./National Radio Astronomy Observatory. Pulsar research at UBC is supported by an NSERC

Discovery Grant and by CIFAR. K.Cr. is supported by a UBC Four Year Fellowship (6456). M.E.D. acknowledges support from the Naval Research Laboratory by NASA under contract S-15633Y. T.D. and M.T.L. are supported by an NSF Astronomy and Astrophysics Grant (AAG) award number 2009468. E.C.F. is supported by NASA under award number 80GSFC21M0002. G.E.F., S.C.S., and S.J.V. are supported by NSF award PHY-2011772. K.A.G. and S.R.T. acknowledge support from an NSF CAREER award #2146016. The work of N.La., X.S., and D.W. is partly supported by the George and Hannah Bolinger Memorial Fund in the College of Science at Oregon State University. N.La. acknowledges the support from Larry W. Martin and Joyce B. O'Neill Endowed Fellowship in the College of Science at Oregon State University. Part of this research was carried out at the Jet Propulsion Laboratory, California Institute of Technology, under a contract with the National Aeronautics and Space Administration (80NM0018D0004). D.R.L. and M.A.M. are supported by NSF #1458952. M.A.M. is supported by NSF #2009425. C.M.F.M. was supported in part by the National Science Foundation under Grants No. NSF PHY-1748958 and AST-2106552. The Dunlap Institute is funded by an endowment estab-

lished by the David Dunlap family and the University of Toronto. K.D.O. was supported in part by NSF Grant No. 2207267. T.T.P. acknowledges support from the Extragalactic Astrophysics Research Group at Eötvös Loránd University, funded by the Eötvös Loránd Research Network (ELKH), which was used during the development of this research. H.A.R. is supported by NSF Partnerships for Research and Education in Physics (PREP) award No. 2216793. S.M.R. and I.H.S. are CIFAR Fellows. Portions of this work performed at NRL were supported by ONR 6.1 basic research funding. J.D.R. also acknowledges support from start-up funds from Texas Tech University. J.S. is supported by an NSF Astronomy and Astrophysics Postdoctoral Fellowship under award AST-2202388, and acknowledges previous support by the NSF under award 1847938. C.U. acknowledges support from BGU (Kreitman fellowship), and the Council for Higher Education and Israel Academy of Sciences and Humanities (Excellence fellowship). C.A.W. acknowledges support from CIERA, the Adler Planetarium, and the Brinson Foundation through a CIERA-Adler postdoctoral fellowship. O.Y. is supported by the National Science Foundation Graduate Research Fellowship under Grant No. DGE-2139292.

-
- [1] Z. Arzoumanian *et al.* (NANOGrav), The NANOGrav 12.5 yr Data Set: Search for an Isotropic Stochastic Gravitational-wave Background, *Astrophys. J. Lett.* **905**, L34 (2020), arXiv:2009.04496 [astro-ph.HE].
- [2] B. Goncharov *et al.*, On the Evidence for a Common-spectrum Process in the Search for the Nanohertz Gravitational-wave Background with the Parkes Pulsar Timing Array, *Astrophys. J. Lett.* **917**, L19 (2021), arXiv:2107.12112 [astro-ph.HE].
- [3] S. Chen *et al.* (EPTA), Common-red-signal analysis with 24-yr high-precision timing of the European Pulsar Timing Array: inferences in the stochastic gravitational-wave background search, *Mon. Not. Roy. Astron. Soc.* **508**, 4970 (2021), arXiv:2110.13184 [astro-ph.HE].
- [4] J. Antoniadis *et al.*, The International Pulsar Timing Array second data release: Search for an isotropic gravitational wave background, *Mon. Not. Roy. Astron. Soc.* **510**, 4873 (2022), arXiv:2201.03980 [astro-ph.HE].
- [5] G. Agazie *et al.* (NANOGrav), The NANOGrav 15 yr Data Set: Evidence for a Gravitational-wave Background, *Astrophys. J. Lett.* **951**, L8 (2023), arXiv:2306.16213 [astro-ph.HE].
- [6] J. Antoniadis *et al.* (EPTA, InPTA), The second data release from the European Pulsar Timing Array - III. Search for gravitational wave signals, *Astron. Astrophys.* **678**, A50 (2023), arXiv:2306.16214 [astro-ph.HE].
- [7] D. J. Reardon *et al.*, Search for an Isotropic Gravitational-wave Background with the Parkes Pulsar Timing Array, *Astrophys. J. Lett.* **951**, L6 (2023), arXiv:2306.16215 [astro-ph.HE].
- [8] H. Xu *et al.*, Searching for the Nano-Hertz Stochastic Gravitational Wave Background with the Chinese Pulsar Timing Array Data Release I, *Res. Astron. Astrophys.* **23**, 075024 (2023), arXiv:2306.16216 [astro-ph.HE].
- [9] R. w. Hellings and G. s. Downs, UPPER LIMITS ON THE ISOTROPIC GRAVITATIONAL RADIATION BACKGROUND FROM PULSAR TIMING ANALYSIS, *Astrophys. J. Lett.* **265**, L39 (1983).
- [10] G. Agazie *et al.* (NANOGrav), The NANOGrav 15 yr Data Set: Constraints on Supermassive Black Hole Binaries from the Gravitational-wave Background, *Astrophys. J. Lett.* **952**, L37 (2023), arXiv:2306.16220 [astro-ph.HE].
- [11] J. Antoniadis *et al.* (EPTA, InPTA), The second data release from the European Pulsar Timing Array - IV. Implications for massive black holes, dark matter, and the early Universe, *Astron. Astrophys.* **685**, A94 (2024), arXiv:2306.16227 [astro-ph.CO].
- [12] J. Ellis, M. Fairbairn, G. Hütsi, J. Raidal, J. Urrutia, V. Vaskonen, and H. Veermäe, Gravitational waves from supermassive black hole binaries in light of the NANOGrav 15-year data, *Phys. Rev. D* **109**, L021302 (2024), arXiv:2306.17021 [astro-ph.CO].
- [13] M. C. Begelman, R. D. Blandford, and M. J. Rees, Massive black hole binaries in active galactic nuclei, *Nature* **287**, 307 (1980).
- [14] M. Milosavljevic and D. Merritt, The Final parsec problem, *AIP Conf. Proc.* **686**, 201 (2003), arXiv:astro-ph/0212270.
- [15] A. Gould and H.-W. Rix, Binary black hole mergers from planet-like migrations, *Astrophys. J. Lett.* **532**, L29 (2000), arXiv:astro-ph/9912111.
- [16] P. J. Armitage and P. Natarajan, Accretion during the merger of supermassive black holes, *Astrophys. J. Lett.* **567**, L9 (2002), arXiv:astro-ph/0201318.
- [17] G. D. Quinlan, The dynamical evolution of massive black hole binaries - I. hardening in a fixed stellar background,

- New Astron. **1**, 35 (1996), arXiv:astro-ph/9601092.
- [18] M. Milosavljevic and D. Merritt, Formation of galactic nuclei, *Astrophys. J.* **563**, 34 (2001), arXiv:astro-ph/0103350.
- [19] M. Enoki and M. Nagashima, The Effect of Orbital Eccentricity on Gravitational Wave Background Radiation from Cosmological Binaries, *Prog. Theor. Phys.* **117**, 241 (2007), arXiv:astro-ph/0609377.
- [20] S. Chen, A. Sesana, and W. Del Pozzo, Efficient computation of the gravitational wave spectrum emitted by eccentric massive black hole binaries in stellar environments, *Mon. Not. Roy. Astron. Soc.* **470**, 1738 (2017), arXiv:1612.00455 [astro-ph.CO].
- [21] J. Raidal, J. Urrutia, V. Vaskonen, and H. Veermäe, Eccentricity effects on the SMBH GW background, (2024), arXiv:2406.05125 [astro-ph.CO].
- [22] J. F. Navarro, C. S. Frenk, and S. D. M. White, The Structure of cold dark matter halos, *Astrophys. J.* **462**, 563 (1996), arXiv:astro-ph/9508025.
- [23] P. Gondolo and J. Silk, Dark matter annihilation at the galactic center, *Phys. Rev. Lett.* **83**, 1719 (1999), arXiv:astro-ph/9906391.
- [24] R. Genzel, F. Eisenhauer, and S. Gillessen, The Galactic Center Massive Black Hole and Nuclear Star Cluster, *Rev. Mod. Phys.* **82**, 3121 (2010), arXiv:1006.0064 [astro-ph.GA].
- [25] S. Chandrasekhar, Dynamical Friction. I. General Considerations: the Coefficient of Dynamical Friction, *Astrophys. J.* **97**, 255 (1943).
- [26] D. Merritt and M. Milosavljevic, Dynamics of dark matter cusps, in *4th International Heidelberg Conference on Dark Matter in Astro and Particle Physics* (2002) pp. 79–89, arXiv:astro-ph/0205140.
- [27] A. Sesana and F. M. Khan, Scattering experiments meet N-body – I. A practical recipe for the evolution of massive black hole binaries in stellar environments, *Mon. Not. Roy. Astron. Soc.* **454**, L66 (2015), arXiv:1505.02062 [astro-ph.GA].
- [28] J. Frank and M. J. Rees, Effects of massive central black holes on dense stellar systems, *Mon. Not. Roy. Astron. Soc.* **176**, 633 (1976).
- [29] E. S. Phinney, A Practical theorem on gravitational wave backgrounds, (2001), arXiv:astro-ph/0108028.
- [30] P. C. Peters and J. Mathews, Gravitational radiation from point masses in a Keplerian orbit, *Phys. Rev.* **131**, 435 (1963).
- [31] A. Sesana, Self consistent model for the evolution of eccentric massive black hole binaries in stellar environments: implications for gravitational wave observations, *Astrophys. J.* **719**, 851 (2010), arXiv:1006.0730 [astro-ph.CO].
- [32] L. Sampson, N. J. Cornish, and S. T. McWilliams, Constraining the Solution to the Last Parsec Problem with Pulsar Timing, *Phys. Rev. D* **91**, 084055 (2015), arXiv:1503.02662 [gr-qc].
- [33] L. Z. Kelley, L. Blecha, L. Hernquist, A. Sesana, and S. R. Taylor, The Gravitational Wave Background from Massive Black Hole Binaries in Illustris: spectral features and time to detection with pulsar timing arrays, *Mon. Not. Roy. Astron. Soc.* **471**, 4508 (2017), arXiv:1702.02180 [astro-ph.HE].
- [34] E. Bortolas, A. Franchini, M. Bonetti, and A. Sesana, The Competing Effect of Gas and Stars in the Evolution of Massive Black Hole Binaries, *Astrophys. J. Lett.* **918**, L15 (2021), arXiv:2108.13436 [astro-ph.HE].
- [35] P. C. Peters, Gravitational Radiation and the Motion of Two Point Masses, *Phys. Rev.* **136**, B1224 (1964).
- [36] A. Ghoshal and A. Strumia, Probing the Dark Matter density with gravitational waves from super-massive binary black holes, *JCAP* **02**, 054, arXiv:2306.17158 [astro-ph.CO].
- [37] Z.-Q. Shen, G.-W. Yuan, Y.-Y. Wang, and Y.-Z. Wang, Dark Matter Spike surrounding Supermassive Black Holes Binary and the nanohertz Stochastic Gravitational Wave Background, (2023), arXiv:2306.17143 [astro-ph.HE].
- [38] M. Aghaie, G. Armando, A. Dondarini, and P. Pani, Bounds on ultralight dark matter from NANOGrav, *Phys. Rev. D* **109**, 103030 (2024), arXiv:2308.04590 [astro-ph.CO].
- [39] L. Hu, R.-G. Cai, and S.-J. Wang, Distinctive GWBs from eccentric inspiraling SMBH binaries with a DM spike, (2023), arXiv:2312.14041 [gr-qc].
- [40] F. M. Khan, A. Just, and D. Merritt, Efficient Merger of Binary Supermassive Black Holes in Merging Galaxies, *Astrophys. J.* **732**, 89 (2011), arXiv:1103.0272 [astro-ph.CO].
- [41] M. Preto, I. Berentzen, P. Berczik, and R. Spurzem, Fast coalescence of massive black hole binaries from mergers of galactic nuclei: implications for low-frequency gravitational-wave astrophysics, *Astrophys. J. Lett.* **732**, L26 (2011), arXiv:1102.4855 [astro-ph.GA].
- [42] F. M. Khan, M. Preto, P. Berczik, I. Berentzen, A. Just, and R. Spurzem, Mergers of Unequal Mass Galaxies: Supermassive Black Hole Binary Evolution and Structure of Merger Remnants, *Astrophys. J.* **749**, 147 (2012), arXiv:1202.2124 [astro-ph.CO].
- [43] D. Merritt and M. Y. Poon, Chaotic loss cones, black hole fueling and the m-sigma relation, *Astrophys. J.* **606**, 788 (2004), arXiv:astro-ph/0302296.
- [44] C. J. Harris and K. Gültekin, Connecting core galaxy properties to the massive black hole binary population, *Monthly Notices of the Royal Astronomical Society* **528**, 1 (2023).
- [45] D. Merritt, Black holes and galaxy evolution, *ASP Conf. Ser.* **197**, 221 (2000), arXiv:astro-ph/9910546.
- [46] M. Celoria, R. Oliveri, A. Sesana, and M. Mapelli, Lecture notes on black hole binary astrophysics (2018) arXiv:1807.11489 [astro-ph.GA].
- [47] W. Dehnen, A Family of Potential-Density Pairs for Spherical Galaxies and Bulges, *Mon. Not. Roy. Astron. Soc.* **265**, 250 (1993).
- [48] S. R. Taylor, J. Simon, and L. Sampson, Constraints On The Dynamical Environments Of Supermassive Black-hole Binaries Using Pulsar-timing Arrays, *Phys. Rev. Lett.* **118**, 181102 (2017), arXiv:1612.02817 [astro-ph.GA].
- [49] S. Chen, A. Sesana, and C. J. Conselice, Constraining astrophysical observables of Galaxy and Supermassive Black Hole Binary Mergers using Pulsar Timing Arrays, *Mon. Not. Roy. Astron. Soc.* **488**, 401 (2019), arXiv:1810.04184 [astro-ph.GA].
- [50] Y.-C. Bi, Y.-M. Wu, Z.-C. Chen, and Q.-G. Huang, Implications for the supermassive black hole binaries from the NANOGrav 15-year data set, *Sci. China Phys. Mech. Astron.* **66**, 120402 (2023), arXiv:2307.00722 [astro-ph.CO].
- [51] D. E. McLaughlin, Evidence in virgo for the universal

- dark matter halo, *Astrophys. J. Lett.* **512**, L9 (1999), [arXiv:astro-ph/9812242](#).
- [52] D. Merritt, The Distribution of Stars and Stellar Remnants at the Galactic Center, *Astrophys. J.* **718**, 739 (2010), [arXiv:0909.1318 \[astro-ph.GA\]](#).
- [53] P. Ullio, H. Zhao, and M. Kamionkowski, A Dark matter spike at the galactic center?, *Phys. Rev. D* **64**, 043504 (2001), [arXiv:astro-ph/0101481](#).
- [54] A. Weltman *et al.*, Fundamental physics with the Square Kilometre Array, *Publ. Astron. Soc. Austral.* **37**, e002 (2020), [arXiv:1810.02680 \[astro-ph.CO\]](#).
- [55] A. Vallenari, The future of astrometry in space, *Frontiers in Astronomy and Space Sciences* **5**, 11 (2018).
- [56] M. Çalıřkan, Y. Chen, L. Dai, N. Anil Kumar, I. Stomberg, and X. Xue, Dissecting the stochastic gravitational wave background with astrometry, *JCAP* **05**, 030, [arXiv:2312.03069 \[gr-qc\]](#).
- [57] C. Tiede and D. J. D’Orazio, Eccentric binaries in retrograde discs, *Mon. Not. Roy. Astron. Soc.* **527**, 6021 (2023), [arXiv:2307.03775 \[astro-ph.GA\]](#).
- [58] A. J. Dittmann, G. Ryan, and M. C. Miller, The Decoupling of Binaries from Their Circumbinary Disks, *Astrophys. J. Lett.* **949**, L30 (2023), [arXiv:2303.16204 \[astro-ph.HE\]](#).
- [59] Z. Haiman, Z. Haiman, B. Kocsis, B. Kocsis, K. Menou, and K. Menou, The Population of Viscosity- and Gravitational Wave-Driven Supermassive Black Hole Binaries Among Luminous AGN, *Astrophys. J.* **700**, 1952 (2009), [Erratum: *Astrophys. J.* 937, 129 (2022)], [arXiv:0904.1383 \[astro-ph.CO\]](#).
- [60] C. Roedig and A. Sesana, Migration of massive black hole binaries in self-gravitating discs: retrograde versus prograde, *Mon. Not. Roy. Astron. Soc.* **439**, 3476 (2014), [arXiv:1307.6283 \[astro-ph.HE\]](#).
- [61] A. Franchini, A. Sesana, and M. Dotti, Circumbinary disc self-gravity governing supermassive black hole binary mergers, *Mon. Not. Roy. Astron. Soc.* **507**, 1458 (2021), [arXiv:2106.13253 \[astro-ph.HE\]](#).
- [62] D. Ayzenberg *et al.*, Fundamental Physics Opportunities with the Next-Generation Event Horizon Telescope, (2023), [arXiv:2312.02130 \[astro-ph.HE\]](#).
- [63] D. J. D’Orazio and M. Charisi, Observational Signatures of Supermassive Black Hole Binaries, *arXiv e-prints*, [arXiv:2310.16896 \(2023\)](#), [arXiv:2310.16896 \[astro-ph.HE\]](#).
- [64] G. Alonso-Álvarez, J. M. Cline, and C. Dewar, Self-Interacting Dark Matter Solves the Final Parsec Problem of Supermassive Black Hole Mergers, *Phys. Rev. Lett.* **133**, 021401 (2024), [arXiv:2401.14450 \[astro-ph.CO\]](#).
- [65] I. Dutra, P. Natarajan, and D. Gilman, Self-Interacting Dark Matter, Core Collapse and the Galaxy-Galaxy Strong Lensing Discrepancy, (2024), [arXiv:2406.17024 \[astro-ph.CO\]](#).
- [66] T. Ikeda, L. Bernard, V. Cardoso, and M. Zilhão, Black hole binaries and light fields: Gravitational molecules, *Phys. Rev. D* **103**, 024020 (2021), [arXiv:2010.00008 \[gr-qc\]](#).
- [67] T. Broadhurst, C. Chen, T. Liu, and K.-F. Zheng, Binary Supermassive Black Holes Orbiting Dark Matter Solitons: From the Dual AGN in UGC4211 to NanoHertz Gravitational Waves, (2023), [arXiv:2306.17821 \[astro-ph.HE\]](#).
- [68] H. Koo, D. Bak, I. Park, S. E. Hong, and J.-W. Lee, Final parsec problem of black hole mergers and ultralight dark matter, *Phys. Lett. B* **856**, 138908 (2024), [arXiv:2311.03412 \[astro-ph.GA\]](#).
- [69] B. C. Bromley, P. Sandick, and B. Shams Es Haghi, Supermassive black hole binaries in ultralight dark matter, *Phys. Rev. D* **110**, 023517 (2024), [arXiv:2311.18013 \[astro-ph.GA\]](#).
- [70] J. C. Aurrekoetxea, K. Clough, J. Bamber, and P. G. Ferreira, Effect of Wave Dark Matter on Equal Mass Black Hole Mergers, *Phys. Rev. Lett.* **132**, 211401 (2024), [arXiv:2311.18156 \[gr-qc\]](#).
- [71] J. C. Aurrekoetxea, J. Marsden, K. Clough, and P. G. Ferreira, Self-interacting scalar dark matter around binary black holes, *Phys. Rev. D* **110**, 083011 (2024), [arXiv:2409.01937 \[gr-qc\]](#).
- [72] L. Z. Kelley, L. Blecha, and L. Hernquist, Massive Black Hole Binary Mergers in Dynamical Galactic Environments, *Mon. Not. Roy. Astron. Soc.* **464**, 3131 (2017), [arXiv:1606.01900 \[astro-ph.HE\]](#).
- [73] A. Sesana, F. Haardt, and P. Madau, Interaction of massive black hole binaries with their stellar environment. I. Ejection of hypervelocity stars, *Astrophys. J.* **651**, 392 (2006), [arXiv:astro-ph/0604299](#).
- [74] E. Vasiliev, F. Antonini, and D. Merritt, The Final-parsec Problem in the Collisionless Limit, *Astrophys. J.* **810**, 49 (2015), [arXiv:1505.05480 \[astro-ph.GA\]](#).
- [75] F. Fastidio, A. Gualandris, A. Sesana, E. Bortolas, and W. Dehnen, Eccentricity evolution of PTA sources from cosmological initial conditions, *Mon. Not. Roy. Astron. Soc.* **532**, 295 (2024), [arXiv:2406.02710 \[astro-ph.GA\]](#).
- [76] E. A. Huerta, S. T. McWilliams, J. R. Gair, and S. R. Taylor, Detection of eccentric supermassive black hole binaries with pulsar timing arrays: Signal-to-noise ratio calculations, *Phys. Rev. D* **92**, 063010 (2015), [arXiv:1504.00928 \[gr-qc\]](#).
- [77] A. Sesana, A. Vecchio, and C. N. Colacino, The stochastic gravitational-wave background from massive black hole binary systems: implications for observations with Pulsar Timing Arrays, *Mon. Not. Roy. Astron. Soc.* **390**, 192 (2008), [arXiv:0804.4476 \[astro-ph\]](#).
- [78] G. Agazie *et al.* (NANOGrav), The NANOGrav 15 yr Data Set: Bayesian Limits on Gravitational Waves from Individual Supermassive Black Hole Binaries, *Astrophys. J. Lett.* **951**, L50 (2023), [arXiv:2306.16222 \[astro-ph.HE\]](#).
- [79] W. G. Lamb and S. R. Taylor, Spectral Variance in a Stochastic Gravitational-wave Background from a Binary Population, *Astrophys. J. Lett.* **971**, L10 (2024), [arXiv:2407.06270 \[gr-qc\]](#).
- [80] G. Sato-Polito and M. Zaldarriaga, The distribution of the gravitational-wave background from supermassive black holes, (2024), [arXiv:2406.17010 \[astro-ph.CO\]](#).
- [81] X. Xue, Z. Pan, and L. Dai, Non-Gaussian Statistics of Nanohertz Stochastic Gravitational Waves, (2024), [arXiv:2409.19516 \[astro-ph.CO\]](#).
- [82] A. S. Hamers, An Improved Numerical Fit to the Peak Harmonic Gravitational Wave Frequency Emitted by an Eccentric Binary, *Res. Notes AAS* **5**, 275 (2021), [arXiv:2111.08033 \[gr-qc\]](#).
- [83] V. Saeedzadeh, S. Mukherjee, A. Babul, M. Tremmel, and T. R. Quinn, Shining light on the hosts of the nanohertz gravitational wave sources: a theoretical perspective, *Mon. Not. Roy. Astron. Soc.* **529**, 4295 (2024), [arXiv:2309.08683 \[astro-ph.GA\]](#).
- [84] M. R. Sah, S. Mukherjee, V. Saeedzadeh, A. Babul,

- M. Tremmel, and T. R. Quinn, Imprints of supermassive black hole evolution on the spectral and spatial anisotropy of nano-hertz stochastic gravitational-wave background, *Mon. Not. Roy. Astron. Soc.* **533**, 1568 (2024), [arXiv:2404.14508 \[astro-ph.CO\]](#).
- [85] A. Sesana, Insights into the astrophysics of supermassive black hole binaries from pulsar timing observations, *Class. Quant. Grav.* **30**, 224014 (2013), [arXiv:1307.2600 \[astro-ph.CO\]](#).
- [86] A. Sesana, F. Shankar, M. Bernardi, and R. K. Sheth, Selection bias in dynamically measured supermassive black hole samples: consequences for pulsar timing arrays, *Mon. Not. Roy. Astron. Soc.* **463**, L6 (2016), [arXiv:1603.09348 \[astro-ph.GA\]](#).
- [87] P. Schechter, An analytic expression for the luminosity function for galaxies, *Astrophys. J.* **203**, 297 (1976).
- [88] P. Lang *et al.*, Bulge Growth and Quenching since $z = 2.5$ in CANDELS/3D-HST, *Astrophys. J.* **788**, 11 (2014), [arXiv:1402.0866 \[astro-ph.GA\]](#).
- [89] A. F. L. Bluck, J. T. Mendel, S. L. Ellison, J. Moreno, L. Simard, D. R. Patton, and E. Starkeburg, Bulge mass is king: The dominant role of the bulge in determining the fraction of passive galaxies in the Sloan Digital Sky Survey, *Mon. Not. Roy. Astron. Soc.* **441**, 599 (2014), [arXiv:1403.5269 \[astro-ph.GA\]](#).
- [90] A. Mitridate, D. Wright, R. von Eckardstein, T. Schröder, J. Nay, K. Olum, K. Schmitz, and T. Trickle, PTArcade, (2023), [arXiv:2306.16377 \[hep-ph\]](#).
- [91] W. G. Lamb, S. R. Taylor, and R. van Haasteren, Rapid refitting techniques for Bayesian spectral characterization of the gravitational wave background using pulsar timing arrays, *Phys. Rev. D* **108**, 103019 (2023), [arXiv:2303.15442 \[astro-ph.HE\]](#).

Supplemental Material: Galaxy Tomography with Gravitational Wave Background from Supermassive Black Hole Binaries

V. Evolution of Eccentric Orbits

We investigate the orbital evolution of supermassive black hole binaries (SMBHBs) driven by both three-body ejection of stars and dark matter (DM), and gravitational wave (GW) emission. In addition to the formalism presented in the main text, our analysis incorporates eccentric orbits with evolving eccentricity. The coupled equations that govern the semi-major axis a and eccentricity e are as follows:

$$\begin{aligned}\frac{da(e, a)}{dt} &= -\frac{64 G^3 M^3}{5} \frac{q}{c^5 a^3} \frac{1}{(1+q)^2} \frac{(1 + \frac{73}{24}e^2 + \frac{37}{96}e^4)}{(1-e^2)^{7/2}} - HG \frac{\rho_i}{\sigma_i} a^2, \\ \frac{de(e, a)}{dt} &= -\frac{304 G^3 M^3}{15} \frac{q}{c^5 a^4} \frac{1}{(1+q)^2} \frac{e(1 + \frac{121}{304}e^2)}{(1-e^2)^{5/2}} + HK(e, a)G \frac{\rho_i}{\sigma_i} a.\end{aligned}\tag{S1}$$

The first terms on the right-hand side of these equations correspond to GW emission [30], while the second terms describe the effects of three-body ejections [17]. Here, G denotes the gravitational constant, M the total mass of the SMBHB, $q \leq 1$ the mass ratio of its components, and ρ_i and σ_i the matter density and velocity dispersion at the SMBHB influence radius r_i , respectively. The dimensionless parameters H and K represent the hardening and eccentricity growth rates, respectively, derived from scattering experiments. For hard binaries, H values typically range from 15 to 20 [17]; in this study, we have fixed H at 18. The function for K is approximated by [17, 73–75]:

$$K(e, a) \approx 0.3e (1 - e^2)^{0.6} \left(1 + \frac{a}{0.2 a_h}\right)^{-1},\tag{S2}$$

which becomes most effective when a is within the hardening radius $a_h \equiv r_i q / (4(1+q)^2)$.

Each evolutionary case begins at the influence radius, r_i , determined by solving the relation $\int_0^{r_i} \rho 4\pi r^2 dr = 2M$ [28] for a power-law distribution $\rho(r) = \rho_{\text{pc}}(r/1 \text{ pc})^{-\gamma}$ prior to disruption. Consequently, $\rho_i \equiv \rho(r_i)$ and $\sigma_i \equiv \sigma(r_i) = \sqrt{GM/r_i}$ are calculated. The initial eccentricity, e_0 , defined at r_i , serves as a fit parameter to be constrained.

We vary both the initial eccentricity, e_0 , and the density profile parameters (ρ_{pc}, γ). We then calculate the orbital evolution for the SMBHB with parameters (M, q) from the determined r_i . The stochastic gravitational wave background (SGWB) spectrum is subsequently calculated by integrating over the SMBHB population parameters (M, q, z), considering the density distribution $d^3\eta/(dz dM dq)$, as referenced in [19, 29, 76]:

$$h_c^2(f) = \frac{4G}{c^2 \pi f} \int dz dM dq \frac{d^3\eta}{dz dM dq} \frac{dE_{\text{GW}}}{df_s} \Big|_{f_s=(1+z)f}.\tag{S3}$$

In this calculation, we neglect Poisson fluctuations in the SMBHB distribution, which have a minor impact on the lowest frequency bins of the NANOGrav 15-year dataset [77–81].

The GW emission spectrum, $dE_{\text{GW}}/d \ln f_s$, calculated at the source frame frequency f_s , includes contributions from various orbital frequencies $f_{\text{orb}}^n = f_s/n$ for integer $n > 0$. It is expressed as [30]:

$$\left. \frac{dE_{\text{GW}}}{df_s} \right|_{f_s=(1+z)f} = \sum_{n=1}^{+\infty} \left. \frac{dE_{\text{GW}}^n/dt}{n df_{\text{orb}}^n/dt} \right|_{f_{\text{orb}}^n=(1+z)f/n}, \quad (\text{S4})$$

where

$$\begin{aligned} \frac{dE_{\text{GW}}^n}{dt} &= \frac{32G^4 M^5}{5c^5 a^5} \frac{q^2}{(1+q)^4} g(n, e), \\ \frac{df_{\text{orb}}^n}{dt} &= -\frac{3\sqrt{GM}}{4\pi a^{5/2}} \frac{da}{dt}. \end{aligned} \quad (\text{S5})$$

The orbital frequency is related to a via Kepler's law $a^3 = GM/(2\pi f_{\text{orb}}^n)^2$. The function $g(n, e)$, defined as

$$\begin{aligned} g(n, e) &= \frac{n^4}{32} \left[\left\{ J_{n-2}(ne) - 2eJ_{n-1}(ne) + \frac{2}{n}J_n(ne) + 2eJ_{n+1}(ne) - J_{n+2}(ne) \right\}^2 \right. \\ &\quad \left. + (1-e^2) \left\{ J_{n-2}(ne) - 2J_n(ne) + J_{n+2}(ne) \right\}^2 + \frac{4}{3n^2} J_n^2(ne) \right], \end{aligned} \quad (\text{S6})$$

converges to $g(2, 0) = 1$ for circular orbits. Here, J_n denotes the Bessel function of the first kind of order n .

In practice, we employ several methods to enhance the efficiency of numerical computation. In Eq. (S4), we apply a cutoff to the summation over n , neglecting all contributions for $n > n_{\text{max}}$, with $n_{\text{max}} = 3n_{\text{peak}}(e_{\text{max}})$. The value of $n_{\text{peak}}(e)$ is given by [82]:

$$n_{\text{peak}}(e) \approx 2 \left(1 + \sum_{k=1}^4 c_k e^k \right) (1-e^2)^{-3/2}, \quad (\text{S7})$$

where $c_1 = -1.01678$, $c_2 = 5.57372$, $c_3 = -4.9271$, and $c_4 = 1.68506$ and e_{max} represents the maximum eccentricity throughout the orbital evolution. Additionally, when n_{max} exceeds 100, we sum the contributions for $n > 101$ using logarithmic steps (i.e., $n = 101, 102, 104, 108, \dots$) and implement numerical integration over n using `numpy.trapz`.

VI. Supermassive Black Hole Binary Population

This section details the semi-analytic SMBHB population model utilized in this study, characterized by the comoving volumetric number density of SMBHBs, $d^3\eta/(dz dM dq)$, alongside astrophysical priors on its normalization. To generate the initial SMBHB population before binary evolution, we use the `holodeck` code, following NANOGrav's astrophysical interpretation paper [10]. However, we replaced the phenomenological environmental prescription [10, 12, 32, 83, 84] with the three-body scattering prescription detailed in Sec. V.

The semi-analytic model is predicated on galaxy merger rates, the SMBH-host galaxy relationship, and cosmological expansion, and is parameterized as follows [85, 86]:

$$\frac{d^3\eta}{dz dM dq} = \frac{d^3\eta_{\text{gal-gal}}}{dz dm_{\star 1} dq_{\star}} \frac{dm_{\star 1}}{dM} \frac{dq_{\star}}{dq}, \quad (\text{S8})$$

where $d^3\eta_{\text{gal-gal}}/(dz dm_{\star 1} dq_{\star})$ represents the volumetric galaxy merger rate density as a function of redshift z , the stellar mass of the primary galaxy $m_{\star 1}$, and the mass ratio of the galaxies $q_{\star} \leq 1$. The galaxy merger rate can be expressed [49]:

$$\frac{d^3\eta_{\text{gal-gal}}}{dz dm_{\star 1} dq_{\star}} = \frac{\Psi(m_{\star 1}, z')}{m_{\star 1} \ln(10)} \frac{P(m_{\star 1}, q_{\star}, z')}{T_{\text{gal-gal}}(m_{\star 1}, q_{\star}, z')} \frac{dt}{dz'}. \quad (\text{S9})$$

Here, $\Psi(m_{\star 1}, z')$ represents the galaxy stellar mass function (GSMF), $P(m_{\star 1}, q_{\star}, z')$ denotes the galaxy pair fraction (GPF), and $T_{\text{gal-gal}}(m_{\star 1}, q_{\star}, z')$ refers to the galaxy merger timescale (GMT). The variable z' is defined as the advanced redshift satisfying $t(z) - t(z') = T_{\text{gal-gal}}(z')$, with the current epoch at $t(0) = 13.79$ Gyr. The rate of change in cosmic time with respect to redshift, dt/dz , is calculated as $1/((1+z)H(z))$, following the standard cosmological model where the Hubble parameter $H(z) = H_0 [\Omega_{\Lambda} + (1+z)^3\Omega_m]^{1/2}$ with $H_0 = 67.4 \text{ km s}^{-1} \text{ Mpc}^{-1}$, $\Omega_m = 0.315$, and $\Omega_{\Lambda} = 0.685$. The terms $dm_{\star 1}/dM$ and dq_{\star}/dq are derived from the SMBH-host relation.

Below, we detail the relevant parameters in the semi-analytic model:

- Galaxy Stellar Mass Function (GSMF) $\Psi(m_{\star 1}, z)$: This function describes the distribution of primary galaxy masses $m_{\star 1}$ at different redshifts z , following the Schechter function [87]:

$$\Psi(m_{\star 1}, z) = \ln(10)\Psi_0 \left(\frac{m_{\star 1}}{M_\psi}\right)^{\alpha_\psi} \exp\left(-\frac{m_{\star 1}}{M_\psi}\right), \quad (\text{S10})$$

where

$$\begin{aligned} \log_{10}(\Psi_0/\text{Mpc}^{-3}) &= \psi_0 + \psi_z \cdot z, \\ \log_{10}(M_\psi/M_\odot) &= m_{\psi,0} + m_{\psi,z} \cdot z, \\ \alpha_\psi &= 1 + \alpha_{\psi,0} + \alpha_{\psi,z} \cdot z. \end{aligned} \quad (\text{S11})$$

- Galaxy Pair Fraction (GPF) $P(m_{\star 1}, q_\star, z)$: This parameterizes the relative number of observable galaxy pairs to total galaxies, following [49]:

$$P(m_{\star 1}, q_\star, z) = P_0 \left(\frac{m_{\star 1}}{10^{11}M_\odot}\right)^{\alpha_p} (1+z)^{\beta_p} q_\star^{\gamma_p}, \quad (\text{S12})$$

where

$$\begin{aligned} \alpha_p &= \alpha_{p,0} + \alpha_{p,z} \cdot z, \\ \gamma_p &= \gamma_{p,0} + \gamma_{p,z} \cdot z. \end{aligned} \quad (\text{S13})$$

- Galaxy Merger Timescale (GMT) $T_{\text{gal-gal}}(m_{\star 1}, q_\star, z)$: This provides the duration for two galaxies to merge, expressed as [49]:

$$T_{\text{gal-gal}}(m_{\star 1}, q_\star, z) = T_0 \left(\frac{m_{\star 1}}{10^{11}M_\odot/h}\right)^{\alpha_t} (1+z)^{\beta_t} q_\star^{\gamma_t}, \quad (\text{S14})$$

where

$$\begin{aligned} \alpha_t &= \alpha_{t,0} + \alpha_{t,z} \cdot z, \\ \gamma_t &= \gamma_{t,0} + \gamma_{t,z} \cdot z. \end{aligned} \quad (\text{S15})$$

- SMBH–host relation: This assumes a one-to-one correspondence between galaxy pairs and SMBHBs as per Ref. [10], expressed as

$$\log_{10}(M_{\text{BH}}/M_\odot) = \mu + \alpha_\mu \log_{10}\left(\frac{M_{\text{bulge}}}{10^{11}M_\odot}\right) + \mathcal{N}(0, \epsilon_\mu), \quad (\text{S16})$$

where $\mathcal{N}(0, \epsilon_\mu)$ denotes a normal distribution accounting for scatter with a mean of zero and standard deviation ϵ_μ in dex. The bulge mass is calculated as a fraction of the total galaxy stellar mass, $M_{\text{bulge}} = f_{\star, \text{bulge}} \cdot m_{\star 1}$, with $f_{\star, \text{bulge}} = 0.615$ [88, 89].

In Table I, we list all the relevant parameters along with their fiducial values and astrophysical priors, as outlined in Ref. [10]. The fiducial values for ψ_0 , $m_{\psi,0}$, μ , and ϵ_μ are based on the best-fit results from the ‘Phenom+Astro’ model. In this study, the comoving volumetric number density of SMBHBs follows these fiducial values. The differential distribution of the fiducial model is shown in Fig.S1.

For the data analysis, we allow the overall normalization of h_c^2 to vary as a nuisance parameter, denoted by N , which accounts for uncertainties in the population model. This parameter is assigned a prior based on the astrophysical priors listed in Table I that contribute to the normalization. Specifically, for each case, we calculate the corresponding h_c^2 for circular orbits driven solely by GW emission, and compare it to that of the fiducial model, defining the ratio as N . The distribution of N is shown in Fig. S2, which can be modeled as $\log_{10} N = \mathcal{N}(-1.46, 1.09)$.

VII. Statistics

In our data analysis, we estimate the posterior distribution of $\log_{10} \rho_{\text{pc}}$, γ , e_0 and $\log_{10} N$. This can be separated into two components:

$$\begin{aligned} &P\left(\log_{10} \frac{\rho_{\text{pc}}/10^5}{M_\odot/\text{pc}^3}, \gamma, e_0, \log_{10} N | \delta t\right) \\ &= \int \prod_k d \log_{10} h_c^2(f_k) P\left(\log_{10} \frac{\rho_{\text{pc}}/10^5}{M_\odot/\text{pc}^3}, \gamma, e_0, \log_{10} N | \{\log_{10} h_c^2(f_k)\}\right) \times P(\{\log_{10} h_c^2(f_k)\} | \delta t), \end{aligned} \quad (\text{S17})$$

| Model Component | Symbol | Fiducial Value | Astrophysical Priors |
|--|----------------------|----------------|-------------------------------|
| GSMF (Ψ) | ψ_0 | -2.27 | $\mathcal{N}(-2.56, 0.4)$ |
| | ψ_z | -0.60 | ... |
| | $m_{\psi,0}$ | 11.15 | $\mathcal{N}(10.9, 0.4)$ |
| | $m_{\psi,z}$ | +0.11 | ... |
| | $\alpha_{\psi,0}$ | -1.21 | $\mathcal{N}(-1.2, 0.2)$ |
| | $\alpha_{\psi,z}$ | -0.03 | ... |
| GPF (P) | P_0 | +0.033 | ... |
| | $\alpha_{p,0}$ | 0.0 | ... |
| | $\alpha_{p,z}$ | 0.0 | ... |
| | $\beta_{p,0}$ | +1.0 | $\mathcal{N}(0.8, 0.4)$ |
| | $\beta_{p,z}$ | 0.0 | ... |
| | $\gamma_{p,0}$ | 0.0 | $\mathcal{N}(0.5, 0.3)$ |
| | $\gamma_{p,z}$ | 0.0 | ... |
| GMT ($T_{\text{gal-gal}}$) | T_0 | +0.5 Gyr | $U(0.2, 5.0)$ Gyr |
| | $\alpha_{t,0}$ | 0.0 | ... |
| | $\alpha_{t,z}$ | 0.0 | ... |
| | $\beta_{t,0}$ | -0.5 | $U(-2.0, 0.0)$ |
| | $\beta_{t,z}$ | 0.0 | ... |
| | $\gamma_{t,0}$ | -1.0 | ... |
| | $\gamma_{t,z}$ | 0.0 | ... |
| $M_{\text{BH}}-M_{\text{bulge}}$ (M_{BH}) | μ | 8.65 | $\mathcal{N}(8.6, 0.2)$ |
| | α_μ | +1.10 | $\mathcal{N}(1.2, 0.2)$ |
| | ϵ_μ | 0.32 | $\mathcal{N}(0.32, 0.15)$ dex |
| | $f_{*,\text{bulge}}$ | +0.615 | ... |

TABLE I: Fiducial values and astrophysical priors for relevant parameters of the semi-analytic model, following Ref. [10]. The fiducial values for ψ_0 , $m_{\psi,0}$, μ , and ϵ_μ are based on the best-fit values from the ‘Phenom+Astro’ model. \mathcal{N} denotes a normal distribution, while U denotes a uniform distribution.

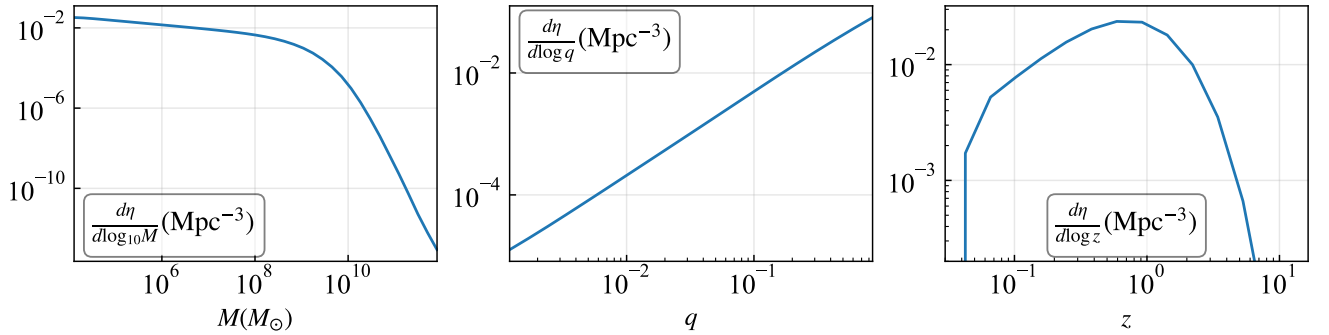


FIG. S1: Comoving volumetric number density of SMBHBs for the fiducial model as a function of total SMBH mass M (left), mass ratio q (middle), and redshift z (right).

where δt represents the timing residual data from the NANOGrav 15-year dataset [5], and $f_k = k/T_{\text{obs}}$ denotes the frequencies indexed by $k = 1, 2, 3, 4, 5$, corresponding to the five lowest frequency bins, with $T_{\text{obs}} \approx 16$ years as the observation time.

The second term in Eq. (S17) represents the posterior distributions of the free spectrum GWs derived by the NANOGrav collaboration [10]. The first term is calculated using Bayes’ theorem:

$$\begin{aligned}
 & P \left(\log_{10} \frac{\rho_{\text{pc}}/10^5}{M_{\odot}/\text{pc}^3}, \gamma, e_0, \log_{10} N | \{ \log_{10} h_c^2(f_k) \} \right) \\
 & \propto P \left(\{ \log_{10} h_c^2(f_k) \} | \log_{10} \frac{\rho_{\text{pc}}/10^5}{M_{\odot}/\text{pc}^3}, \gamma, e_0, \log_{10} N \right) P \left(\log_{10} \frac{\rho_{\text{pc}}/10^5}{M_{\odot}/\text{pc}^3} \right) P(\gamma) P(e_0) P(N),
 \end{aligned} \tag{S18}$$

The first term is computed in Sec. V, where Poisson fluctuations are neglected. The remaining terms are the priors

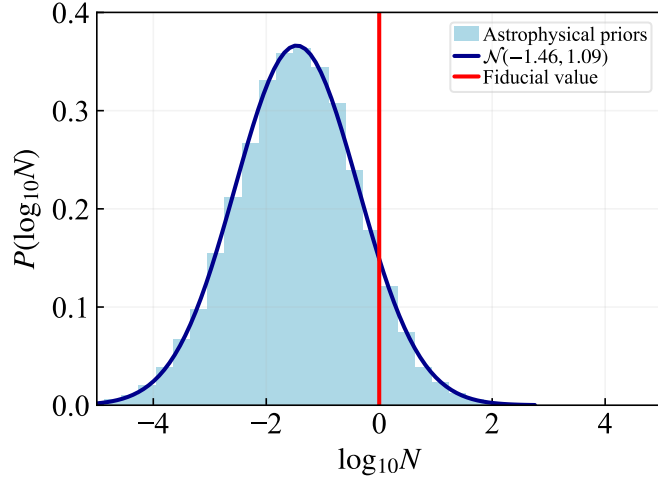


FIG. S2: Distribution of the normalization factor N , defined as the ratio between the h_c^2 magnitude resulting from SMBHB population models (based on astrophysical priors) and the fiducial value in Table I, without accounting for environmental hardening and eccentricities. The distribution is fit as $\log_{10} N = \mathcal{N}(-1.46, 1.08)$, and used as the prior for normalization in data analysis. The fiducial value, fixed at $N = 1$, is shown by the red line.

for each parameter:

$$\begin{aligned}
 P\left(\log_{10} \frac{\rho_{\text{pc}}/10^5}{M_{\odot}/\text{pc}^3}\right) &= U[-4, 4], \\
 P(\gamma) &= U[0, 2.4], \\
 P(e_0) &= U[0, 0.999], \\
 P(N) &= \mathcal{N}(-1.46, 1.09).
 \end{aligned}
 \tag{S19}$$

where the prior for N is calculated in Sec. VI.

For practical implementation, we use `PTArcade` [90], based on `ceffy1` [91], to model the prior distributions and fit the results to the free spectrum data.